

LETTER TO THE EDITOR

# The mass-metallicity relation of high- $z$ type-2 active galactic nuclei

K. Matsuoka<sup>1,2</sup>, T. Nagao<sup>3</sup>, A. Marconi<sup>1</sup>, R. Maiolino<sup>4,5</sup>, F. Mannucci<sup>2</sup>, G. Cresci<sup>2</sup>, K. Terao<sup>6</sup>, and H. Ikeda<sup>7</sup>

<sup>1</sup> Dipartimento di Fisica e Astronomia, Università degli Studi di Firenze, Via G. Sansone 1, I-50019 Sesto Fiorentino, Italy

<sup>2</sup> INAF – Osservatorio Astrofisico di Arcetri, Largo Enrico Fermi 5, I-50125 Firenze, Italy

e-mail: matsuoka@arcetri.astro.it

<sup>3</sup> Research Center for Space and Cosmic Evolution, Ehime University, 2-5 Bunkyo-cho, Matsuyama 790-8577, Japan

<sup>4</sup> Cavendish Laboratory, University of Cambridge, 19 J. J. Thomson Avenue, Cambridge CB3 0HE, UK

<sup>5</sup> Kavli Institute for Cosmology, University of Cambridge, Madingley Road, Cambridge CB3 0HA, UK

<sup>6</sup> Graduate School of Science and Engineering, Ehime University, 2-5 Bunkyo-cho, Matsuyama 790-8577, Japan

<sup>7</sup> National Astronomical Observatory of Japan (NAOJ), 2-21-1 Osawa, Mitaka, Tokyo 181-8588, Japan

## ABSTRACT

The mass-metallicity relation (MZR) of type-2 active galactic nuclei (AGNs) at  $1.2 < z < 4.0$  is investigated by using high- $z$  radio galaxies (HzRGs) and X-ray selected radio-quiet AGNs. We combine new rest-frame ultraviolet (UV) spectra of two radio-quiet type-2 AGNs obtained with FOCAS on the Subaru Telescope with existing rest-frame UV emission lines, i.e., C IV  $\lambda$ 1549, He II  $\lambda$ 1640, and C III  $\lambda$ 1909, of a sample of 16 HzRGs and 6 additional X-ray selected type-2 AGNs, whose host stellar masses have been estimated in literature. We divided our sample in three stellar mass bins and calculated averaged emission-line flux ratios of C IV  $\lambda$ 1549/He II  $\lambda$ 1640 and C III  $\lambda$ 1909/C IV  $\lambda$ 1549. Comparing observed emission-line flux ratios with photoionization model predictions, we estimated narrow line region (NLR) metallicities for each mass bin. We found that there is a positive correlation between NLR metallicities and stellar masses of type-2 AGNs at  $z \sim 3$ . This is the first indication that AGN metallicities are related to their hosts, i.e., stellar mass. Since NLR metallicities and stellar masses follow a similar relation as the MZR in star-forming galaxies at similar redshifts, our results indicate that NLR metallicities are related to those of the host galaxies. This study highlights the importance of considering lower-mass X-ray selected AGNs in addition to radio galaxies to explore the metallicity properties of NLRs at high redshift.

**Key words.** galaxies: active – galaxies: evolution – galaxies: nuclei – quasars: emission lines – quasars: general

## 1. Introduction

Metallicity provides one of the most important clues in understanding galaxy formation and evolution since metal formation and enrichment are closely connected with the past star formation history in galaxies. Generally, the metallicity of star-forming galaxies is obtained by using various emission lines at the rest-frame optical wavelengths (e.g., [O II]  $\lambda$ 3727, H $\beta$ , [O III]  $\lambda$ 5007, H $\alpha$ , and [N II]  $\lambda$ 6584), emitted in H II regions (e.g., Nagao et al. 2006a; Curti et al. 2017). The relationship between mass of galaxies and their metal (the so-called mass-metallicity relation, MZR) has been investigated for about forty years (Lequeux et al. 1979). By using Sloan Digital Sky Survey (SDSS) imaging and spectroscopy of  $\sim 53,000$  star-forming galaxies at  $z \sim 0.1$ , Tremonti et al. (2004) made a major step forward in this field by obtaining a highly statistically sound relationship between stellar mass and gas-phase oxygen abundances in galaxies (see also Kewley & Ellison 2008; Hayashi et al. 2009; Andrews & Martini 2013). Furthermore, this correlation has been explored at high redshifts, up to  $z \sim 3$ , and a clear evolution with cosmological time, has been reported (e.g., Savaglio et al. 2005; Maiolino et al. 2008; Mannucci et al. 2009; Cresci et al. 2012; Yuan et al. 2013; Hunt et al. 2016; Onodera et al. 2016; Suzuki et al. 2017).

The metallicity of star-forming galaxies at high redshift has been estimated through deep near-infrared spectroscopy. However, since the emission lines for the metallicity diagnostics shift out of the  $K$ -band atmospheric window for galaxies at  $z > 3.5$ , studies are more challenging for higher- $z$  galaxies re-

quiring space-based spectrograph. An alternative approach to investigate the metallicity in the early universe is to focus on active galactic nuclei (AGNs) instead of star-forming galaxies. Thanks to their high luminosity and strong emission lines in the wide wavelength range from the ultraviolet (UV) to the infrared, arising from gas clouds photoionized by their central accreting black hole, it is possible to measure the metallicity even in high- $z$  universe. Since Hamann & Ferland (1992) proposed that broad-line region (BLR) metallicities ( $Z_{\text{BLR}}$ ) can be estimated from N V  $\lambda$ 1240, C IV  $\lambda$ 1549, and He II  $\lambda$ 1640 lines (see also Hamann & Ferland 1993, 1999), AGN metallicities have been studied extensively. By measuring emission-line flux ratios of SDSS quasars, i.e., N V  $\lambda$ 1240/C IV  $\lambda$ 1549, (Si IV  $\lambda$ 1398+O IV  $\lambda$ 1402)/C IV  $\lambda$ 1549, Al III  $\lambda$ 1857/C IV  $\lambda$ 1549, and N V  $\lambda$ 1240/He II  $\lambda$ 1640, Nagao et al. (2006b) investigated BLR metallicities and their properties. Based on a spectral stacking analysis, they found a positive correlation between BLR metallicities and AGN luminosities ( $L_{\text{AGN}}$ ): more luminous quasars show more metal-rich BLR clouds (see also Hamann & Ferland 1993; Juarez et al. 2009). By using SDSS spectra of 2383 quasars at  $2.3 < z < 3.0$ , Matsuoka et al. (2011) revealed that the observed  $L_{\text{AGN}}-Z_{\text{BLR}}$  trend is mostly a consequence of the relation between black-hole mass ( $M_{\text{BH}}$ ) and BLR metallicity. This result indicates that AGN host galaxies may follow a MZR given the relation between black-hole mass and galaxy mass. However, it is unclear if the BLR metallicities trace chemical properties of their host galaxies, since AGN broad lines originate from a very small region in galactic nuclei,  $R_{\text{BLR}} < 1$  pc (e.g.,

arXiv:1807.09276v1 [astro-ph.GA] 24 Jul 2018

Suganuma et al. 2006), which may have evolved more rapidly and may not be representative of the metallicity in their host galaxies.

To investigate the metallicity on the scale of AGN host galaxies, the narrow line region (NLR) has been studied, since the typical NLR size is comparable to the size of their host galaxies,  $R_{\text{NLR}} \sim 10^{1-4}$  pc (e.g., Bennert et al. 2006b,a). Furthermore, NLR masses are usually  $\sim 10^{4-8} M_{\odot}$ , much larger than those of the BLR,  $\sim 10^{2-4} M_{\odot}$  (e.g., Baldwin et al. 2003). Thus, NLR metallicities allow us to investigate chemical properties at host galaxy scales. However, since it has been difficult to discover type-2 quasars in the high- $z$  universe, the NLR metallicity at  $z > 1$  have been investigated only with high- $z$  radio galaxies (HzRGs) in previous studies. Nagao et al. (2006c) studied NLR metallicities of 51 HzRGs at  $1.2 < z < 3.8$  with a metallicity diagnostic diagram involving C IV  $\lambda 1549$ , He II  $\lambda 1640$ , and C III]  $\lambda 1909$ . They reported that HzRGs do not show any redshift evolution of NLR metallicity: a lack of redshift evolution is similar to that seen for the BLR metallicities (Nagao et al. 2006b; Juarez et al. 2009). Matsuoka et al. (2009) confirmed the absence of any significant NLR metallicity evolution up to  $z \sim 4$  by observing nine HzRGs at  $z > 2.7$ . Moreover, Matsuoka et al. (2011) found that the most distant radio galaxy, TN J0924–2201 at  $z = 5.19$ , has already experienced significant chemical evolution.

On the other hand, Matsuoka et al. (2009) also found a positive correlation between NLR metallicities and AGN luminosities, as for the BLR metallicities. This may be originated from the galaxy mass-metallicity relation, if we assume  $L_{\text{AGN}} \propto M_{\text{BH}} \propto M_{\text{host}}$ . However, there is still no direct evidence that NLR metallicities are related to their host properties, and in particular with their stellar mass ( $M_{\star}$ ). In this letter, we focus on HzRGs and X-ray selected type-2 AGNs at  $1.2 < z < 4.0$  and investigate their NLR metallicities, adopting a diagnostic diagram of C IV  $\lambda 1549$ , He II  $\lambda 1640$ , and C III]  $\lambda 1909$  emission lines. Thus, by collecting their stellar masses from the recent literature we examine their dependence on NLR metallicities.

## 2. Observations and Data from the Literature

In order to study NLR metallicities, we utilize type-2 AGNs, i.e. in which the BLR and strong continuum emission are obscured allowing us accurate measurements of narrow-line emission. First, we focus on HzRG samples (e.g., De Breuck et al. 2000) which have been identified as type-2 AGNs at high redshift with radio observations: e.g., ultra-steep-spectrum radio sources with radio spectral index  $\alpha < -1.30$  ( $S_{\nu} \propto \nu^{\alpha}$ ) are adopted as efficient HzRG tracers in De Breuck et al. (2000) and over 160 sources are identified as HzRGs at  $0 < z < 5.2$  with devoted optical spectroscopic observations. Requiring that C IV  $\lambda 1549$ , He II  $\lambda 1640$ , and C III]  $\lambda 1909$  lines are detected, 67 HzRGs at  $1.2 < z < 4.0$  are collected from Nagao et al. (2006c), Bornancini et al. (2007), and Matsuoka et al. (2009, 2011). We listed these emission-line fluxes in Table 1.

As inferred from the tight correlation in the Hubble  $K$ - $z$  diagram (e.g., De Breuck et al. 2002), HzRGs are usually associated with very massive elliptical galaxies ( $M_{\star} > 10^{11} M_{\odot}$ ; e.g., Seymour et al. 2007). In order to also sample the lower stellar mass range, in this study we also focus on X-ray selected type-2 AGNs which have been discovered in recent observations. First, we obtained optical spectra of two X-ray selected radio-quiet type-2 AGNs at  $z > 3.0$  in the Cosmic Evolution Survey (COSMOS) field (Mainieri et al. 2011) with FOCAS (the Faint Object Camera And Spectrograph; Kashikawa et al. 2002)

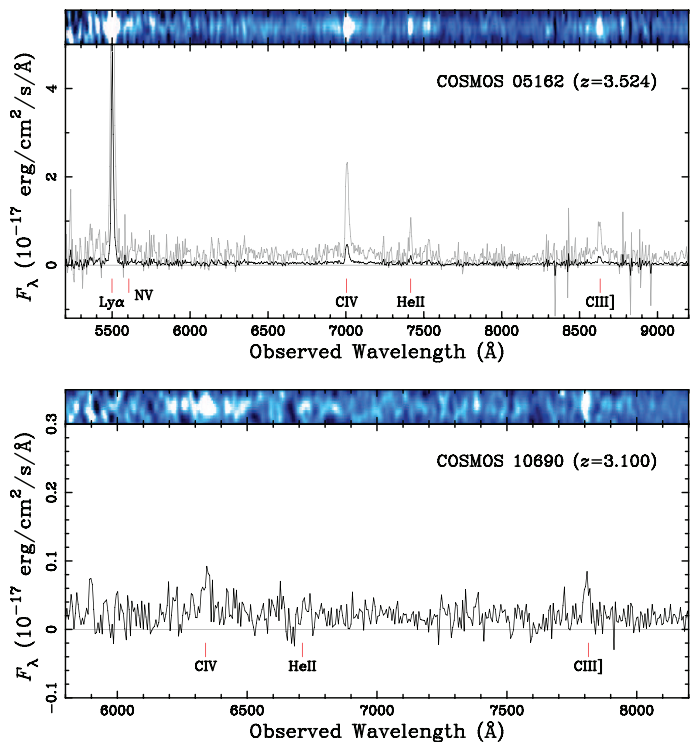


**Fig. 1.** Reduced spectra of two X-ray selected type-2 AGNs in the COSMOS field (ID: 05162 and 10690) obtained with FOCAS, after adopting 4-pixel binning in wavelength direction. Their two-dimensional spectra with a 2'1 section are shown at the top, respectively. Red vertical lines indicate the central wavelengths of rest-frame UV emission lines, i.e., Ly $\alpha$ , N V  $\lambda 1240$ , C IV  $\lambda 1549$ , He II  $\lambda 1640$ , and C III]  $\lambda 1909$ . The grey line in the *top* panel is an arbitrary spectrum with five times the flux for recognising relatively weak emission lines.

at the Subaru Telescope (24–25 December 2013). Observations were performed with the 300R dispersion element and SY47 filter to cover the wavelength range of  $\lambda_{\text{obs}} = 4900 - 9500 \text{ \AA}$ . We used a slit width of 0".6. Standard data reduction procedures were applied to these spectra by using IRAF tasks. Figure 1 shows the final reduced spectra. We measured emission-line fluxes of detected lines by fitting them with a Gaussian function using the IRAF task *splot* (see Table 1). For undetected lines,  $3\sigma$  upper limits are given by assuming an averaged line width of 25 Å calculated from the detected lines. Then, we collected emission-line fluxes of 10 X-ray selected AGNs at  $1.5 < z < 4.0$  from Nagao et al. (2006c). Nine of them are X-ray selected type-2 AGNs in the Chandra Deep Field-South (CDF-S) field (Szokoly et al. 2004) and the remaining CXO 52 is a type-2 quasar in the Lynx field identified as a hard X-ray source with *Chandra* (Stern et al. 2002). Emission line fluxes of these 13 X-ray type-2 AGNs are listed in Table 1.

We collected their stellar masses from the literature. Regarding HzRGs, we matched our sample with stellar mass catalogs in Seymour et al. (2007) and De Breuck et al. (2010). Overall, we obtained stellar masses of 21 HzRGs including 8 upper limits. These studies derived stellar masses through a spectral energy distribution (SED) fit based on the *Spitzer* infrared (3.6–160  $\mu\text{m}$ ) data, covering the rest-frame optical to infrared wavelengths (see Seymour et al. 2007, for more detail): De Breuck et al. (2010) followed the procedures of Seymour et al. (2007) with the same method and photometric bands. For X-ray selected AGNs in the COSMOS field, stellar masses are collected from Mainieri et al. (2011). These masses are also derived by SED fitting with mul-

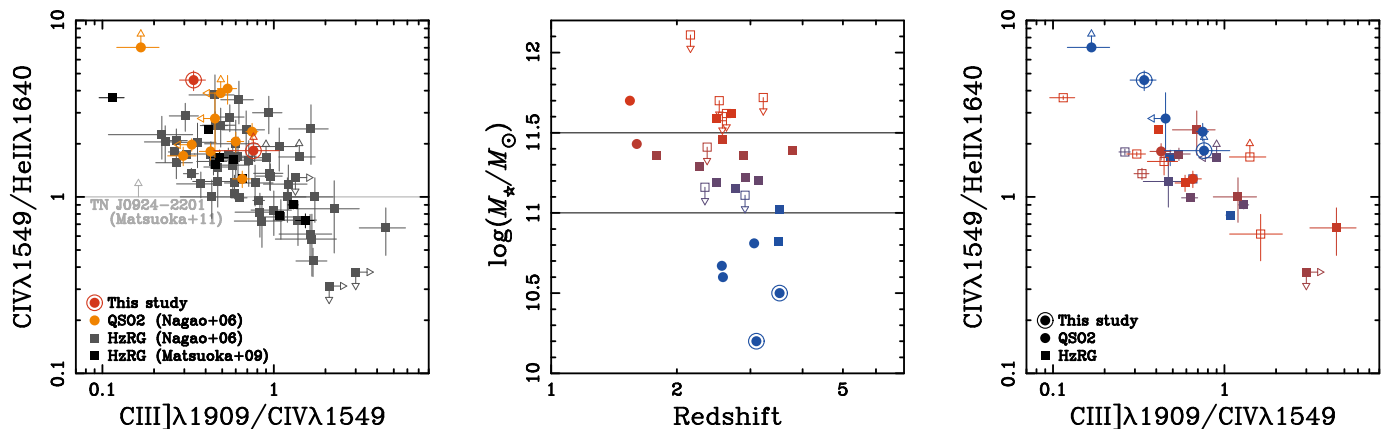


**Fig. 2.** Emission-line flux ratios of high- $z$  type-2 AGNs plotted on the diagnostic diagram of  $C\text{IV}\lambda 1549/\text{HeII}\lambda 1640$  versus  $C\text{III]}\lambda 1909/C\text{IV}\lambda 1549$  (left). Gray- and black-filled squares and arrows denote HzRGs compiled by Nagao et al. (2006c) and Matsuoka et al. (2009), respectively. The  $C\text{IV}\lambda 1549/\text{HeII}\lambda 1640$  lower limit for TN J0924–2201 is shown as a light-gray arrow (Matsuoka et al. 2011). Our new type-2 AGNs are shown as red-filled double circles (COSMOS 05162 and 10690). Orange circles denote X-ray selected type-2 AGNs in Nagao et al. (2006c). The *middle* panel shows the objects in our sample having an estimate of stellar mass as a function of redshift, and their emission-line flux ratios are plotted in the *right* panel. In the *middle* and *right* panels, symbols are same as the *left* panel but color-coded according to the stellar mass: bluer and redder for lower and higher mass objects, respectively. Note that open squares in these panels indicate HzRGs with upper limits of stellar masses.

tiwavelength data set of COSMOS. For five additional AGNs in CDF-S, we adopted stellar masses derived using a tight correlation between rest-frame optical colors and stellar mass-to-light ratios in Xue et al. (2010). Altogether, we obtained stellar masses of 28 type-2 AGNs containing 8 HzRGs with upper limits (see Table 1).

### 3. Result

We calculate emission-line flux ratios of  $C\text{IV}\lambda 1549/\text{HeII}\lambda 1640$  and  $C\text{III]}\lambda 1909/C\text{IV}\lambda 1549$ , that are sensitive to both the NLR gas metallicity and ionization parameter (see Nagao et al. 2006c; Matsuoka et al. 2009). Figure 2 shows our sample plotted on a diagnostic diagram of  $C\text{IV}\lambda 1549$ ,  $\text{HeII}\lambda 1640$ , and  $C\text{III]}\lambda 1909$  lines in the *left* panel. Our new type-2 AGNs are located in the same area as the X-ray selected AGNs in Nagao et al. (2006c). In the *right* panel, 28 type-2 AGNs for which stellar masses were derived are plotted, color-coded according to their masses: we gave the stellar mass distribution as a function of redshift in the *middle* panel. Thanks to X-ray selected type-2 AGNs, we could cover the low- $M_*$  range, i.e.,  $\log(M_*/M_\odot) < 11$ , which could not be explored with HzRGs.

### 4. Discussion

In order to examine the relation between NLR metallicities and stellar masses statistically, we divided the 20 type-2 AGNs whose stellar masses are estimated without upper limits into three subsamples with stellar mass ranges, i.e.,  $\log(M_*/M_\odot) < 11.0$ ,  $11.0 < \log(M_*/M_\odot) < 11.5$ , and  $\log(M_*/M_\odot) > 11.5$  (these intervals are shown with horizontal lines in the *middle* panel in Figure 2). Then, we calculated averaged emission-line flux ratios of  $C\text{IV}\lambda 1549/\text{HeII}\lambda 1640$  and  $C\text{III]}\lambda 1909/C\text{IV}\lambda 1549$  for each subsample: we use 15 objects whose emission-line flux ratios are measured without upper or lower limits (i.e., three, nine, and three objects, respectively). Note that our final sample would not be biased due to the discard of objects with upper or lower limits since the distribution of them show no obvious difference from the original sample (see the *right* panel of Figure 2). Figure 3 shows these averaged flux ratios on the diag-

nostic diagrams (*top* panels). Using these averaged points, we estimate NLR metallicities for each stellar mass.

To estimate NLR metallicities from observational emission-line flux ratios, we carried out model calculations using the photoionization code Cloudy (version 17.00; Ferland et al. 1998, 2017): NLR clouds are mainly photoionized and not significantly affected by shocks when we focus on UV emission lines (see Matsuoka et al. 2009). We assumed three cloud models with hydrogen densities of  $n_{\text{H}} = 10^1$ ,  $10^4$ , and  $10^5 \text{ cm}^{-3}$ . For each model, we calculated emission-line flux ratios by spanning ionization parameter and metallicity in the following ranges  $U = 10^{-3.0} - 10^{-0.4}$  and  $Z_{\text{NLR}} = 0.1 - 10Z_\odot$ , with step values of  $\Delta \log U = 0.2$  and  $\Delta \log(Z_{\text{NLR}}/Z_\odot) = 0.01$ , respectively (i.e., 8442 models in total). We assume a typical AGN SED as photoionizing continuum radiation, using the “table AGN” command in Cloudy (Mathews & Ferland 1987). Chemical compositions of NLR gas clouds are scaled by maintaining solar abundance ratios except for helium and nitrogen. We adopted analytical expressions for He and N relative abundances as a function of metallicities (see Dopita et al. 2000; Russell & Dopita 1992; van Zee et al. 1998). We stopped calculations when the hydrogen ionization fraction dropped below 15%.

Our model predictions of  $C\text{IV}\lambda 1549/\text{HeII}\lambda 1640$  and  $C\text{III]}\lambda 1909/C\text{IV}\lambda 1549$  are overplotted on the diagnostic diagrams (*top* panels of Figure 3): metallicity-constant and  $U$ -constant sequences are denoted as orange and blue lines, respectively. Our models confirm these photoionization models are useful to investigate NLR metallicities, although they show some dependences on hydrogen gas densities. Comparing these model predictions with our  $M_*$ -averaged line ratios we estimated mean NLR metallicities. We show results of  $Z_{\text{NLR}}$  estimates as a function of stellar masses for each  $n_{\text{H}}$  model in bottom panels of Figure 3. We estimated NLR metallicities for each  $M_*$ -averaged line ratio and their errors from averaged emission-line flux ratios and their error bars, respectively, matching them to model calculations with a metallicity step of  $\Delta \log(Z_{\text{NLR}}/Z_\odot) = 0.01$ . Since absolute NLR metallicities are not determined uniquely due to dependences of gas densities, we compare the relative  $Z_{\text{NLR}}$  differences for each density. This approach should be reliable since Sanders et al. (2016) reported

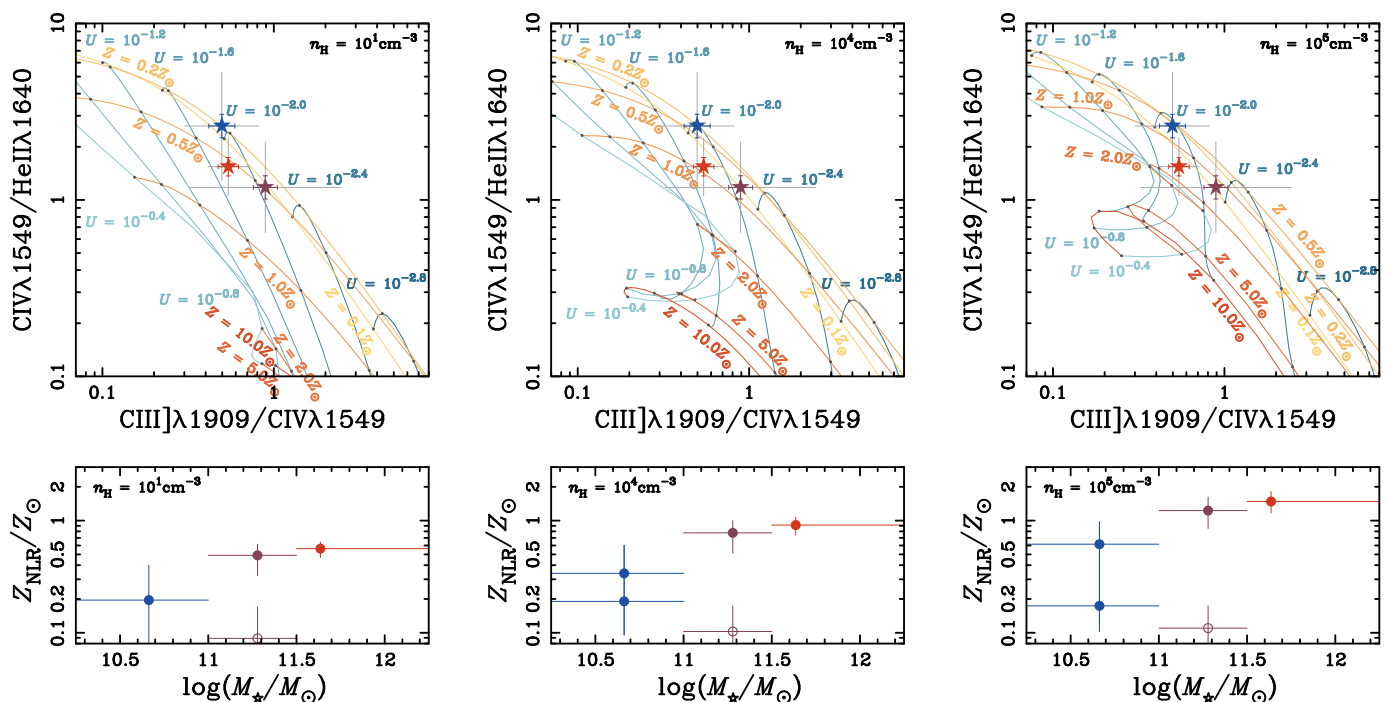


**Fig. 3.** Averaged emission-line flux ratios of low (blue), middle (purple), and high (red) mass subsamples plotted on the diagnostic diagram on C IV  $\lambda$ 1549, He II  $\lambda$ 1640 and C III ] $\lambda$ 1909 (*top* panels). The model predictions with different gas densities ( $\log n_{\text{H}} = 1, 4,$  and  $5$ ) are presented in the *left, middle,* and *right* panels, respectively. Constant metallicity and constant ionization parameter sequences are denoted by orange and blue solid lines, respectively. The gray bars denote the root mean square of the data distribution and the estimated errors in the averaged values are shown as color bars. The *bottom* panels show the NLR metallicities as a function of stellar masses, estimated with different three gas density models. Open circles would be less-likely solutions (see text).

no dependence of gas density on stellar mass investigating the [O II] $\lambda$  $\lambda$ 3726,3729 and/or [S II] $\lambda$  $\lambda$ 6716,6731 doublets of local and high- $z$  star-forming galaxies at  $z \sim 2.3$  (see also Shimakawa et al. 2015; Kaasinen et al. 2017). Note that in principle we derived two values of metallicities if emission-line flux ratios are located in a degenerated area on the model predictions. However, lower metallicity in the middle- $M_{\star}$  bin is unphysical as a significant decrease of metallicity around medium-masses has never been seen for any population of galaxies, at any redshift, and not conceived by any model or cosmological simulation, therefore we exclude such lower metallicities solution in the middle- $M_{\star}$  bin, and consider only the upper solution for this bin.

As shown in these panels of Figure 3, we find positive correlations between NLR metallicities and stellar masses in type-2 AGNs at  $1.2 < z < 4.0$  at different fixed densities. This result is the first indication that AGN gas metallicities are related to their host properties, i.e., host galaxy masses in this case, most likely indicating  $Z_{\text{NLR}} \propto Z_{\text{gal}}$  if we assume that AGN host galaxies have the same MZR in the star-forming galaxies. We thus propose that NLR metallicity is correlated with host metallicity, although additional data sets would be needed to confirm this statistically.

The same averaged emission-line flux ratios shown in *top* panels of Figure 3 may also be reproduced if there is an anti-correlation between stellar masses and densities instead of the MZR. However, some observational studies of star-forming galaxies at  $0 < z < 2.5$  indicated that electron densities do not show any such dependence on stellar masses. For example, Kaasinen et al. (2017) found no significant  $M_{\star}$ - $n_e$  trend of star-forming galaxies at  $z \sim 1.5$  although local SDSS galaxies indicate a weak positive correlation between electron den-

sity and stellar mass, indicating the opposite sense. Moreover, Shimakawa et al. (2015) reported any correlation between  $M_{\star}$  and  $n_e$  cannot be identified with H $\alpha$ -selected star-forming galaxies at  $z = 2.5$  (see also Sanders et al. 2016). Note here that we assume these  $M_{\star}$ - $n_e$  relation of star-forming galaxies are applicable to NLR densities. Therefore, we conclude that our mass-averaged emission-line flux ratios can be explained mainly by the dependence on NLR metallicities.

Although there are uncertainties associated with density dependences, we compare our MZR of type-2 AGNs with those of galaxies. Figure 4 shows the redshift evolution of the MZRs for star-forming galaxies at  $z = 0.07, 0.7, 2.2,$  and  $3.1$  (Kewley & Ellison 2008; Savaglio et al. 2005; Erb et al. 2006; Mannucci et al. 2009), with our results are overplotted. Since the mean redshift of our sample is  $\sim 2.7$ , we focus on the MZR of star-forming galaxies at  $z = 3.1$  as a comparison. As shown in this figure, we indicate that MZRs obtained with high- $n_{\text{H}}$  models ( $n_{\text{H}} = 10^4$  and  $10^5 \text{ cm}^{-3}$  shown as an orange shaded area) seems consistent with MZR of star-forming galaxies. Recently, Nitta et al. (in prep.) has found that NLR gas densities of high- $z$  AGNs are relatively higher than those of low- $z$  ones. By investigating rest-frame optical emission lines of quasars, they estimated a typical gas density of  $\sim 10^{5.5} \text{ cm}^{-3}$  (see also Araki et al. 2012).

Note that some studies (e.g., Nagao et al. 2006c; Matsuoka et al. 2009) about the chemical evolution of HzRGs claimed that there is no significant metallicity evolution in NLRs, up to  $z \sim 4$ , apparently contradicting our result that HzRGs follow the redshift-dependent MZR of star-forming galaxies. However, a possibility is that it is not possible to identify such redshift evolution only focusing on HzRGs hosted in massive elliptical galaxies. Probably, the inclusion of X-ray

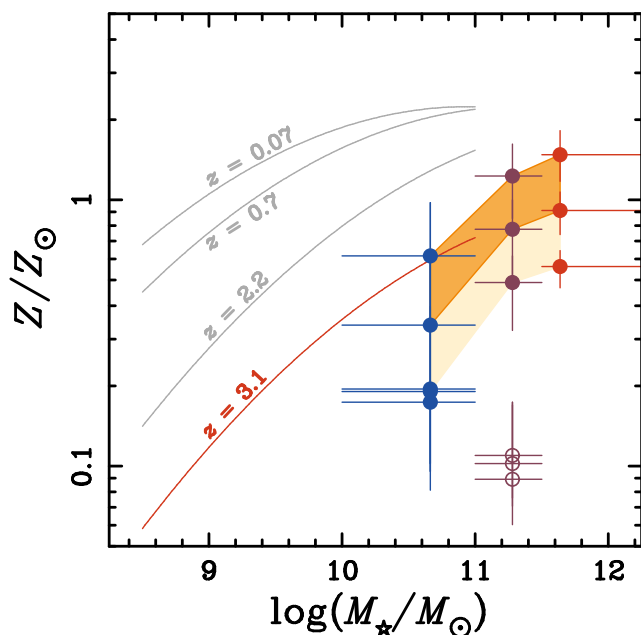


**Fig. 4.** The mass-metallicity relation of type-2 AGNs at  $z \sim 3$  comparing with MZR of star-forming galaxies. Gray solid curves are MZR of star-forming galaxies at  $z = 0.07, 0.7,$  and  $2.2,$  and red curve is for  $z = 3.1$  galaxies in Mannucci et al. (2009). Filled and open circles are same as Figure 3, and the orange area denotes MZR of type-2 AGNs which NLR metallicities are estimated with high- $n_{\text{H}}$  models.

selected AGNs with  $\log(M_*/M_\odot) \sim 10.5$  has helped to reveal such redshift-evolving MZR in type-2 AGNs as shown in this study. Moreover, star formation rate (SFR) or gas mass should be crucial parameters to include, as recent studies have revealed that the relation between stellar mass, gas-phase metallicity, and SFR or gas mass (fundamental metallicity relation: FMR) is important to understand the chemical evolution of galaxies (e.g., Mannucci et al. 2010; Lara-López et al. 2010; Bothwell et al. 2016). To investigate the FMR of type-2 AGNs statistically we need a larger sample and also access to SFR diagnostics that are not affected by the AGN activity, e.g., the far-infrared luminosity (e.g., Beelen et al. 2006; Matsuoka & Woo 2015; Matsuoka & Ueda 2017).

## 5. Conclusion

We have investigated the relation between NLR metallicities and stellar masses of type-2 AGNs at  $1.2 < z < 4.0$  by using a pilot sample of 11 HzRGs and four X-ray selected type-2 AGNs and found the following results:

1. We found indications of a positive correlation between NLR metallicities and stellar masses of type-2 AGNs at  $1.2 < z < 4.0$ ; this is the first direct evidence that AGN metallicities are related to their host properties.
2. Although there are uncertainties associated with the density dependence of the metallicity diagnostic diagrams, we have found that the mass-metallicity relation of type-2 AGNs, as inferred by us, are compatible with that of star-forming galaxies at similar redshifts, indicating that NLR metallicity is connected with host metallicities.

*Acknowledgements.* We would like to thank Takashi Hattori for assisting our FOCAS observations (S13B-019 and S14B-003). We are also grateful to Gray J. Ferland for providing the great photoionization code Cloudy. Data analysis were

in part carried out on common-use data analysis computer system at the Astronomy Data Center, ADC, of the National Astronomical Observatory of Japan (NAOJ). K.M. is supported by Japan Society for the Promotion of Science (JSPS) Overseas Research Fellowships. T.N. is supported by JSPS KAKENHI Grant Nos. 16H01101, 16H03958, and 17H01114. R.M. acknowledges support by the Science and Technology Facilities Council (STFC) and the ERC Advanced Grant 695671 “QUENCH”.

## References

- Andrews, B. H., & Martini, P. 2013, *ApJ*, 765, 140  
 Araki, N., Nagao, T., Matsuoka, K., et al. 2012, *A&A*, 543, A143  
 Baldwin, J. A., Ferland, G. J., Korista, K. T., et al. 2003, *ApJ*, 582, 590  
 Beelen, A., Cox, P., Benford, D. J., et al. 2006, *ApJ*, 642, 694  
 Bennert, N., Jungwiert, B., Komossa, S., et al. 2006, *A&A*, 456, 953  
 Bennert, N., Jungwiert, B., Komossa, S., et al. 2006, *A&A*, 459, 55  
 Bornancini, C. G., De Breuck, C., de Vries, W., et al. 2007, *MNRAS*, 378, 551  
 Bothwell, M. S., Maiolino, R., Ciccone, C., et al. 2016, *A&A*, 595, A48  
 Curti, M., Cresci, G., Mannucci, F., et al. 2017, *MNRAS*, 465, 1384  
 Cresci, G., Mannucci, F., Sommariva, V., et al. 2012, *MNRAS*, 421, 262  
 De Breuck, C., Röttgering, H., Miley, G., et al. 2000, *A&A*, 362, 519  
 De Breuck, C., van Breugel, W., Stanford, S. A., et al. 2002, *AJ*, 123, 637  
 De Breuck, C., Seymour, N., Stern, D., et al. 2010, *ApJ*, 725, 36  
 Dopita, M. A., Kewley, L. J., Heisler, C. A., & Sutherland, R. S. 2000, *ApJ*, 542, 224  
 Erb, D. K., Shapley, A. E., Pettini, M., et al. 2006, *ApJ*, 644, 813  
 Ferland, G. J., Korista, K. T., Verner, D. A., et al. 1998, *PASP*, 110, 761  
 Ferland, G. J., Chatzikos, M., Guzmán, F., et al. 2017, *Rev. Mexicana Astron. Astrofis.*, 53, 385  
 Hamann, F., & Ferland, G. 1992, *ApJ*, 391, L53  
 Hamann, F., & Ferland, G. 1993, *ApJ*, 418, 11  
 Hamann, F., & Ferland, G. 1999, *ARA&A*, 37, 487  
 Hayashi, M., Motohara, K., Shimasaku, K., et al. 2009, *ApJ*, 691, 140  
 Hunt, L., Dayal, P., Magrini, L., & Ferrara, A. 2016, *MNRAS*, 463, 2002  
 Jiang, L., Fan, X., Vestergaard, M., et al. 2007, *AJ*, 134, 1150  
 Juárez, Y., Maiolino, R., Mujica, R., et al. 2009, *A&A*, 494, L25  
 Kaasinen, M., Bian, F., Groves, B., Kewley, L. J., & Gupta, A. 2017, *MNRAS*, 465, 3220  
 Kashikawa, N., Aoki, K., Asai, R., et al. 2002, *PASJ*, 54, 819  
 Kewley, L. J., & Ellison, S. L. 2008, *ApJ*, 681, 1183-1204  
 Lara-López, M. A., Cepa, J., Bongiovanni, A., et al. 2010, *A&A*, 521, L53  
 Lequeux, J., Peimbert, M., Rayo, J. F., et al. 1979, *A&A*, 80, 155  
 Mainieri, V., Bongiorno, A., Merloni, A., et al. 2011, *A&A*, 535, A80  
 Maiolino, R., Nagao, T., Grazian, A., et al. 2008, *A&A*, 488, 463  
 Mannucci, F., Cresci, G., Maiolino, R., et al. 2009, *MNRAS*, 398, 1915  
 Mannucci, F., Cresci, G., Maiolino, R., et al. 2010, *MNRAS*, 408, 2115  
 Mathews, W. G., & Ferland, G. J. 1987, *ApJ*, 323, 456  
 Matsuoka, K., Nagao, T., Maiolino, R., et al. 2009, *A&A*, 503, 721  
 Matsuoka, K., Nagao, T., Marconi, A., et al. 2011, *A&A*, 527, A100  
 Matsuoka, K., Nagao, T., Maiolino, R., et al. 2011, *A&A*, 532, L10  
 Matsuoka, K., & Woo, J.-H. 2015, *ApJ*, 807, 28  
 Matsuoka, K., & Ueda, Y. 2017, *ApJ*, 838, 128  
 Nagao, T., Marconi, A., & Maiolino, R. 2006, *A&A*, 447, 157  
 Nagao, T., Maiolino, R., & Marconi, A. 2006, *A&A*, 447, 863  
 Nagao, T., Maiolino, R., & Marconi, A. 2006, *A&A*, 459, 85  
 Onodera, M., Carollo, C. M., Lilly, S., et al. 2016, *ApJ*, 822, 42  
 Russell, S. C., & Dopita, M. A. 1992, *ApJ*, 384, 508  
 Sanders, R. L., Shapley, A. E., Kriek, M., et al. 2016, *ApJ*, 816, 23  
 Savaglio, S., Glazebrook, K., Le Borgne, D., et al. 2005, *ApJ*, 635, 260  
 Seymour, N., Stern, D., De Breuck, C., et al. 2007, *ApJS*, 171, 353  
 Shimakawa, R., Kodama, T., Steidel, C. C., et al. 2015, *MNRAS*, 451, 1284  
 Stern, D., Moran, E. C., Coil, A. L., et al. 2002, *ApJ*, 568, 71  
 Suganuma, M., Yoshii, Y., Kobayashi, Y., et al. 2006, *ApJ*, 639, 46  
 Suzuki, T. L., Kodama, T., Onodera, M., et al. 2017, *ApJ*, 849, 39  
 Szokoly, G. P., Bergeron, J., Hasinger, G., et al. 2004, *ApJS*, 155, 271  
 Tremonti, C. A., Heckman, T. M., Kauffmann, G., et al. 2004, *ApJ*, 613, 898  
 van Zee, L., Salzer, J. J., & Haynes, M. P. 1998, *ApJ*, 497, L1  
 Xue, Y. Q., Brandt, W. N., Luo, B., et al. 2010, *ApJ*, 720, 368  
 Yuan, T.-T., Kewley, L. J., & Richard, J. 2013, *ApJ*, 763, 9

**Table 1.** Emission-line measurements of type-2 AGNs and their host stellar masses.

Source	$z$	Line Flux [ $10^{-17}$ erg cm $^{-2}$ s $^{-1}$ ]					$\log M_{\star}/M_{\odot}$	Ref. <sup>a</sup>
		Ly $\alpha$	N v $\lambda$ 1240	C iv $\lambda$ 1549	He II $\lambda$ 1640	C III] $\lambda$ 1909		
HzRGs in Nagao et al. (2006c)								
USS 0003–019	1.541	–	–	5.90 $\pm$ 1.20	3.90 $\pm$ 0.80	3.40 $\pm$ 0.50	–	–
MG 0018+0940	1.586	–	–	0.81 $\pm$ 0.16	0.42 $\pm$ 0.08	0.87 $\pm$ 0.17	–	–
WN J0040+3857	2.606	4.10 $\pm$ 0.82	< 0.20	< 1.50	< 0.30	0.60 $\pm$ 0.10	–	–
MG 0046+1102	1.813	–	–	0.65 $\pm$ 0.13	0.55 $\pm$ 0.11	0.79 $\pm$ 0.16	–	–
MG 0122+1923	1.595	–	–	0.32 $\pm$ 0.06	0.38 $\pm$ 0.08	0.32 $\pm$ 0.06	–	–
USS 0200+015	2.229	17.40 $\pm$ 2.20	< 0.40	4.20 $\pm$ 0.50	3.20 $\pm$ 0.40	4.00 $\pm$ 0.50	–	–
USS 0211–122	2.336	5.70 $\pm$ 0.60	1.49 $\pm$ 0.13	2.82 $\pm$ 0.10	1.57 $\pm$ 0.03	0.74 $\pm$ 0.05	< 11.16	DB10
USS 0214+183	2.130	–	–	3.00 $\pm$ 0.30	1.80 $\pm$ 0.20	1.80 $\pm$ 0.20	–	–
WN J0303+3733	2.504	10.30 $\pm$ 2.06	< 0.20	1.50 $\pm$ 0.20	0.50 $\pm$ 0.10	1.40 $\pm$ 0.20	–	–
MG 0311+1532	1.986	–	–	0.34 $\pm$ 0.07	0.20 $\pm$ 0.04	0.21 $\pm$ 0.04	–	–
BRL 0310–150	1.769	–	–	10.20 $\pm$ 1.50	4.00 $\pm$ 0.80	5.00 $\pm$ 0.80	–	–
USS 0355–037	2.153	11.20 $\pm$ 1.80	< 0.30	2.70 $\pm$ 0.60	3.70 $\pm$ 0.70	2.30 $\pm$ 0.50	–	–
USS 0448+091	2.037	12.20 $\pm$ 1.40	< 0.40	1.20 $\pm$ 0.40	1.40 $\pm$ 0.40	2.70 $\pm$ 0.60	–	–
USS 0529–549	2.575	7.40 $\pm$ 0.80	< 0.20	0.40 $\pm$ 0.10	0.60 $\pm$ 0.10	1.80 $\pm$ 0.30	11.46	Se07
4C +41.17	3.792	14.60 $\pm$ 2.92	0.39 $\pm$ 0.08	1.32 $\pm$ 0.26	0.55 $\pm$ 0.11	0.91 $\pm$ 0.18	11.39	Se07
B3 0731+438	2.429	31.00 $\pm$ 6.20	0.71 $\pm$ 0.06	4.65 $\pm$ 0.10	3.04 $\pm$ 0.05	2.12 $\pm$ 0.05	–	–
USS 0748+134	2.419	6.30 $\pm$ 0.80	< 0.20	1.80 $\pm$ 0.30	1.50 $\pm$ 0.30	1.40 $\pm$ 0.30	–	–
USS 0828+193	2.572	13.30 $\pm$ 1.30	3.67 $\pm$ 0.59	18.17 $\pm$ 0.45	10.38 $\pm$ 0.14	5.59 $\pm$ 0.68	< 11.60	DB10
BRL 0851–142	1.665	–	–	3.40 $\pm$ 0.40	2.30 $\pm$ 0.30	1.60 $\pm$ 0.20	–	–
TN J0941–1628	1.644	–	–	3.20 $\pm$ 0.50	0.90 $\pm$ 0.20	2.00 $\pm$ 0.30	–	–
USS 0943–242	2.923	20.10 $\pm$ 2.00	1.12 $\pm$ 0.06	4.65 $\pm$ 0.11	4.71 $\pm$ 0.13	2.93 $\pm$ 0.31	11.22	Se07
MG 1019+0534	2.765	0.84 $\pm$ 0.17	0.23 $\pm$ 0.05	1.04 $\pm$ 0.21	0.85 $\pm$ 0.17	0.49 $\pm$ 0.10	11.15	DB10
TN J1033–1339	2.427	9.80 $\pm$ 1.96	< 0.10	2.30 $\pm$ 0.30	0.80 $\pm$ 0.10	0.70 $\pm$ 0.10	–	–
TN J1102–1651	2.111	2.70 $\pm$ 0.54	< 0.20	1.00 $\pm$ 0.20	1.30 $\pm$ 0.20	1.10 $\pm$ 0.20	–	–
USS 1113–178	2.239	6.40 $\pm$ 0.70	< 0.20	1.70 $\pm$ 0.40	0.70 $\pm$ 0.20	2.80 $\pm$ 0.30	–	–
3C 256	1.824	54.20 $\pm$ 0.70	< 2.70	5.23 $\pm$ 0.08	5.47 $\pm$ 0.05	4.28 $\pm$ 0.33	–	–
USS 1138–262	2.156	13.90 $\pm$ 1.60	< 0.30	0.80 $\pm$ 0.20	1.30 $\pm$ 0.20	1.30 $\pm$ 0.30	< 12.11	Se07
BRL 1140–114	1.935	–	–	1.00 $\pm$ 0.30	0.50 $\pm$ 0.10	0.60 $\pm$ 0.10	–	–
4C +26.38	2.608	–	–	8.90 $\pm$ 1.10	5.70 $\pm$ 0.80	2.40 $\pm$ 0.50	–	–
MG 1251+1104	2.322	2.31 $\pm$ 0.46	< 0.06	0.30 $\pm$ 0.06	0.30 $\pm$ 0.06	0.52 $\pm$ 0.10	–	–
WN J1338+3532	2.769	17.80 $\pm$ 3.56	< 0.60	1.30 $\pm$ 0.20	3.00 $\pm$ 0.30	2.20 $\pm$ 0.30	–	–
MG 1401+0921	2.093	–	–	0.41 $\pm$ 0.08	0.50 $\pm$ 0.10	0.34 $\pm$ 0.07	–	–
3C 294	1.786	155.00 $\pm$ 31.0	3.10 $\pm$ 0.62	15.50 $\pm$ 3.10	15.50 $\pm$ 3.10	18.60 $\pm$ 3.72	11.36	DB10
USS 1410–001	2.363	28.00 $\pm$ 5.60	1.24 $\pm$ 0.12	2.91 $\pm$ 0.20	2.15 $\pm$ 0.05	0.96 $\pm$ 0.07	< 11.41	DB10
BRL 1422–297	1.632	–	–	4.30 $\pm$ 0.60	2.10 $\pm$ 0.40	1.00 $\pm$ 0.20	–	–
USS 1425–148	2.349	20.70 $\pm$ 4.14	< 0.70	2.30 $\pm$ 0.40	2.30 $\pm$ 0.40	1.00 $\pm$ 0.30	–	–
USS 1436+157	2.538	42.00 $\pm$ 4.70	< 0.80	17.00 $\pm$ 1.90	6.00 $\pm$ 0.80	9.40 $\pm$ 1.70	–	–
3C 324	1.208	–	–	3.67 $\pm$ 0.58	2.70 $\pm$ 0.31	3.47 $\pm$ 0.39	–	–
USS 1558–003	2.527	14.90 $\pm$ 1.50	< 0.10	2.70 $\pm$ 0.30	1.70 $\pm$ 0.20	1.20 $\pm$ 0.20	< 11.70	DB10
BRL 1602–174	2.043	–	–	10.00 $\pm$ 1.10	4.80 $\pm$ 0.60	2.70 $\pm$ 0.30	–	–
TXS J1650+0955	2.510	20.90 $\pm$ 4.18	< 0.10	3.20 $\pm$ 0.40	2.70 $\pm$ 0.30	1.20 $\pm$ 0.30	–	–
8C 1803+661	1.610	–	–	5.30 $\pm$ 1.06	2.60 $\pm$ 0.52	1.90 $\pm$ 0.38	–	–
4C 40.36	2.265	–	2.91 $\pm$ 0.56	13.61 $\pm$ 0.51	7.77 $\pm$ 0.56	7.39 $\pm$ 1.18	11.29	Se07
BRL 1859–235	1.430	–	–	3.40 $\pm$ 0.68	4.60 $\pm$ 0.92	4.70 $\pm$ 0.94	–	–
4C 48.48	2.343	–	1.45 $\pm$ 0.40	5.55 $\pm$ 0.05	5.32 $\pm$ 0.35	3.28 $\pm$ 0.10	–	–
MRC 2025–218	2.630	4.00 $\pm$ 0.80	0.62 $\pm$ 0.21	0.69 $\pm$ 0.07	< 0.41	0.97 $\pm$ 0.21	< 11.62	DB10
TXS J2036+0256	2.130	6.80 $\pm$ 1.36	< 0.30	< 0.90	0.70 $\pm$ 0.20	1.20 $\pm$ 0.30	–	–
MRC 2104–242	2.491	57.00 $\pm$ 11.40	< 3.80	3.80 $\pm$ 0.70	< 2.28	< 3.42	11.19	DB10
4C 23.56	2.483	8.00 $\pm$ 1.60	1.15 $\pm$ 0.13	1.80 $\pm$ 0.15	1.50 $\pm$ 0.10	1.06 $\pm$ 0.10	11.59	Se07
MG 2109+0326	1.634	–	–	< 0.10	0.32 $\pm$ 0.06	0.21 $\pm$ 0.04	–	–
MG 2121+1839	1.860	–	–	0.53 $\pm$ 0.11	0.14 $\pm$ 0.03	0.24 $\pm$ 0.05	–	–
USS 2251–089	1.986	0.00 $\pm$ 0.00	0.00 $\pm$ 0.00	3.30 $\pm$ 0.40	1.30 $\pm$ 0.20	1.50 $\pm$ 0.20	–	–
MG 2308+0336	2.457	2.93 $\pm$ 0.59	0.57 $\pm$ 0.11	0.63 $\pm$ 0.13	0.39 $\pm$ 0.08	0.45 $\pm$ 0.09	–	–
4C +28.58	2.891	0.00 $\pm$ 0.00	0.00 $\pm$ 0.00	< 0.60	1.60 $\pm$ 0.40	1.80 $\pm$ 0.40	11.36	DB10
HzRGs in Bornancini et al. (2007)								
MP J0340–6507	2.289	0.40 $\pm$ 0.05	–	0.15 $\pm$ 0.05	0.26 $\pm$ 0.05	0.25 $\pm$ 0.05	–	–
TN J1941–1951	2.667	3.70 $\pm$ 0.40	–	0.90 $\pm$ 0.10	0.40 $\pm$ 0.10	0.20 $\pm$ 0.10	–	–
MP J2352–6154	1.573	–	–	0.70 $\pm$ 0.10	0.40 $\pm$ 0.04	0.30 $\pm$ 0.04	–	–

Table 1. Continued.

Source	$z$	Line Flux [ $10^{-17}$ erg cm $^{-2}$ s $^{-1}$ ]					$\log M_{\star}/M_{\odot}$	Ref. <sup>a</sup>
		Ly $\alpha$	N v $\lambda$ 1240	C IV $\lambda$ 1549	He II $\lambda$ 1640	C III] $\lambda$ 1909		
HzRGs in Matsuoka et al. (2009)								
TN J0121+1320	3.517	1.58 $\pm$ 0.01	< 0.09	0.26 $\pm$ 0.01	0.33 $\pm$ 0.01	0.28 $\pm$ 0.01	11.02	DB10
TN J0205+2242	3.507	8.93 $\pm$ 0.02	< 0.10	0.87 $\pm$ 0.03	0.52 $\pm$ 0.05	0.42 $\pm$ 0.05	10.82	DB10
MRC 0316–257	3.130	2.02 $\pm$ 0.01	< 0.04	0.27 $\pm$ 0.01	0.30 $\pm$ 0.01	0.35 $\pm$ 0.02	11.20	DB10
USS 0417–181	2.773	0.85 $\pm$ 0.02	< 0.10	0.36 $\pm$ 0.03	0.49 $\pm$ 0.02	0.55 $\pm$ 0.05	–	–
TN J0920–0712	2.758	30.50 $\pm$ 0.03	1.02 $\pm$ 0.01	3.37 $\pm$ 0.01	2.06 $\pm$ 0.01	1.95 $\pm$ 0.03	–	–
WN J1123+3141	3.221	1.88 $\pm$ 0.01	1.70 $\pm$ 0.01	1.57 $\pm$ 0.01	0.43 $\pm$ 0.01	0.18 $\pm$ 0.03	< 11.72	DB10
4C +24.28	2.913	4.59 $\pm$ 0.02	1.23 $\pm$ 0.01	1.24 $\pm$ 0.02	0.98 $\pm$ 0.01	0.81 $\pm$ 0.04	< 11.11	DB10
USS 1545–234	2.751	1.76 $\pm$ 0.01	1.34 $\pm$ 0.03	1.34 $\pm$ 0.02	0.88 $\pm$ 0.01	0.61 $\pm$ 0.03	–	–
USS 2202+128	2.705	2.95 $\pm$ 0.01	0.16 $\pm$ 0.02	0.70 $\pm$ 0.01	0.29 $\pm$ 0.01	0.29 $\pm$ 0.01	11.62	DB10
The most distant radio galaxy in Matsuoka et al. (2011)								
TN J0924–2201	5.190	16.10 $\pm$ 0.56	< 1.25	5.46 $\pm$ 0.52	< 5.54	–	–	–
X-ray selected radio-quiet type-2 AGNs in this study								
COSMOS 05162	3.524	76.80 $\pm$ 1.26	< 5.84	11.90 $\pm$ 0.77	2.59 $\pm$ 0.29	4.05 $\pm$ 0.65	10.50	Ma11
COSMOS 10690	3.100	< 12.16	< 6.82	2.25 $\pm$ 0.68	< 1.23	1.71 $\pm$ 0.48	10.20	Ma11
X-ray selected type-2 AGNs in Nagao et al. (2006c)								
CDFS–027	3.064	12.60 $\pm$ 0.70	2.50 $\pm$ 0.70	6.40 $\pm$ 0.50	2.30 $\pm$ 0.90	< 2.90	10.81	Xu10
CDFS–031	1.603	–	–	24.10 $\pm$ 1.40	13.30 $\pm$ 1.20	10.30 $\pm$ 1.30	11.43	Xu10
CDFS–057	2.562	112.20 $\pm$ 1.30	8.40 $\pm$ 1.40	17.80 $\pm$ 0.80	7.60 $\pm$ 0.80	13.30 $\pm$ 0.90	10.67	Xu10
CDFS–112a	2.940	58.30 $\pm$ 0.50	14.60 $\pm$ 0.80	15.20 $\pm$ 1.00	8.90 $\pm$ 0.90	4.50 $\pm$ 0.80	–	–
CDFS–153	1.536	–	–	25.50 $\pm$ 1.40	6.20 $\pm$ 1.10	13.70 $\pm$ 1.60	–	–
CDFS–202	3.700	78.10 $\pm$ 1.00	26.80 $\pm$ 1.10	38.90 $\pm$ 1.10	19.70 $\pm$ 1.50	< 12.90	–	–
CDFS–263b	3.660	70.90 $\pm$ 0.70	4.60 $\pm$ 0.70	15.50 $\pm$ 0.80	< 4.00	< 7.60	–	–
CDFS–531	1.544	–	–	22.00 $\pm$ 1.40	17.40 $\pm$ 1.50	14.40 $\pm$ 1.50	11.70	Xu10
CDFS–901	2.578	37.10 $\pm$ 0.60	6.50 $\pm$ 0.80	19.70 $\pm$ 1.00	< 2.80	3.30 $\pm$ 0.90	10.60	Xu10
CXO 52	3.288	189.00 $\pm$ 4.00	6.00 $\pm$ 1.20	35.00 $\pm$ 2.00	17.00 $\pm$ 2.00	21.00 $\pm$ 2.00	–	–

Notes. <sup>(a)</sup> DB10 = De Breuck et al. (2010); Se07 = Seymour et al. (2007); Ma11 = Mainieri et al. (2011); Xu10 = Xue et al. (2010).